Development of white matter and reading skills

Jason D. Yeatman[a,b,1], Robert F. Dougherty[b], Michal Ben-Shachar[c,d], and Brian A. Wandell[a,b]

[a]Department of Psychology and [b]Stanford Center for Cognitive and Neurobiological Imaging, Stanford University, Stanford, CA 94035; and [c]The Gonda Multidisciplinary Brain Research Center and [d]Department of English, Bar Ilan University, Ramat Gan 52900, Israel

Edited by Marcus E. Raichle, Washington University in St. Louis, St. Louis, MO, and approved September 13, 2012 (received for review April 24, 2012)

White matter tissue properties are highly correlated with reading proficiency; we would like to have a model that relates the dynamics of an individual's white matter development to their acquisition of skilled reading. The development of cerebral white matter involves multiple biological processes, and the balance between these processes differs between individuals. Cross-sectional measures of white matter mask the interplay between these processes and their connection to an individual's cognitive development. Hence, we performed a longitudinal study to measure white-matter development (diffusion-weighted imaging) and reading development (behavioral testing) in individual children (age 7–15 y). The pattern of white-matter development differed significantly among children. In the left arcuate and left inferior longitudinal fasciculus, children with above-average reading skills initially had low fractional anisotropy (FA) that increased over the 3-y period, whereas children with below-average reading skills had higher initial FA that declined over time. We describe a dual-process model of white matter development comprising biological processes with opposing effects on FA, such as axonal myelination and pruning, to explain the pattern of results.

plasticity | neuroprognosis | education | dti | tensor

Reading requires efficient communication within a network of visual, auditory, and language-processing regions that are separated by many centimeters. Hence, the white-matter fascicles that connect these regions are critical for proficient reading (1). Only in the last decade has it become possible to study the microstructural properties of the white matter in the living human brain, and only in recent years has there been an opportunity to trace the developmental progression of these fascicles systematically. During this decade it has been shown that learning to read is associated with corresponding changes in sensory and language circuits in the brain (2–5).

Diffusion measurements of the white-matter pathways (3, 5–7) and neurological case studies (8, 9) suggest that in typical development and education both the left hemisphere arcuate fasciculus and inferior longitudinal fasciculus (ILF) carry signals important for reading. Studies in adults, adolescents, and school-age children have reported differences between good and poor readers in white-matter volume and diffusion properties in the vicinity of these pathways (10–14). One possibility is that these differences are present from an early age, remain constant through development, and constrain children's aptitude for reading. An alternative possibility is that there is an interaction between the biological development and timing of instruction. Two case studies support this hypothesis. When damage to the arcuate fasciculus occurs at birth, normal reading skills can develop (15); when damage to the arcuate fasciculus occurs later, for example after reading instruction has begun, it can result in severe reading impairment (9). These cases suggest that learning depends on the circuits' current state and capacity for plasticity. In this view a child's success in learning to read may require that instruction be delivered during a window of time when the reading circuits are sufficiently developed but still capable of growth.

There have been significant advances in understanding white-matter development using cross-sectional designs (16–19), but understanding the coupling between active developmental processes in the white matter and cognitive development requires following individual children longitudinally as their cognitive skills mature. We followed an initial cohort of 55 children between the ages of 7 and 12 y, longitudinally for 3 y to disambiguate the relationship between white-matter development and the maturation of reading skills. From the initial cohort, 39 children were measured at least three times with diffusion-weighted imaging; cognitive, language, and reading skills were assessed each year with norm-referenced standardized tests.

Results

Identification of Key White-Matter Fascicles. The act of reading can be separated into phonological (auditory) and orthographic (visual) processing that use different neural pathways (20–23). We identified two major white-matter fascicles (Fig. 1) that project to (*a*) regions of cortex involved in phonological manipulations, and (*b*) regions involved in seeing words. The arcuate fasciculus (blue in Fig. 1*C*) is a fiber tract that connects the posterior inferior frontal cortex, including Broca's area, and the lateral temporal cortex, including Wernicke's area. This pathway is important for phonological awareness, an essential skill in reading development (6, 24, 25). The ILF (orange in Fig. 1*C*) is a principal pathway carrying signals between the occipital lobe and the anterior, medial, and inferior temporal lobe. A portion of the ILF projects to the visual word form area (VWFA) in the occipital temporal sulcus (7). The VWFA is considered essential for seeing words (26–28).

Measuring Reading Performance and Brain Development. Although every child's reading proficiency increased from one year to the next, their skills relative to their peers did not change significantly. The rank order correlation of the Woodcock–Johnson Basic Reading standardized scores across measurement years ranged from $r = 0.79$ to $r = 0.89$ (Table 1), similar to the test–retest reliability of the measure (29). Children who had below-average reading abilities at the onset of the study generally remained below average.

Scores on all the reading tests [Test of Word Reading Efficiency (TOWRE), Comprehensive Test of Phonological Processing (CTOPP), Gray Oral Reading Test (GORT), and Woodcock–Johnson] were highly correlated. The main text presents the results for the Woodcock–Johnson Basic Reading Skills standardized scores; results for the other reading measures are reported in *SI Text*, *Covariation Among Reading Measures*.

The stability of the standardized reading scores across the four measurements implies that there is little variation in the rate of reading development across children. Hence each child's performance on the Woodcock–Johnson Basic Reading skills composite index can be summarized with a single score. The main text presents results for children's initial reading performance, but the results remain the same regardless of which year's behavioral measurement are used. The results using the average of the four reading measurements are presented in the *SI Text*.

Author contributions: J.D.Y., R.F.D., M.B.-S., and B.A.W. designed research; J.D.Y., R.F.D., M.B.-S., and B.A.W. performed research; J.D.Y. and R.F.D. contributed new reagents/analytic tools; J.D.Y. and R.F.D. analyzed data; and J.D.Y. and B.A.W. wrote the paper.

The authors declare no conflict of interest.

This article is a PNAS Direct Submission.

[1]To whom correspondence should be addressed. E-mail: jyeatman@stanford.edu.

See Author Summary on page 17756 (volume 109, number 44).

This article contains supporting information online at www.pnas.org/lookup/suppl/doi:10.1073/pnas.1206792109/-/DCSupplemental.

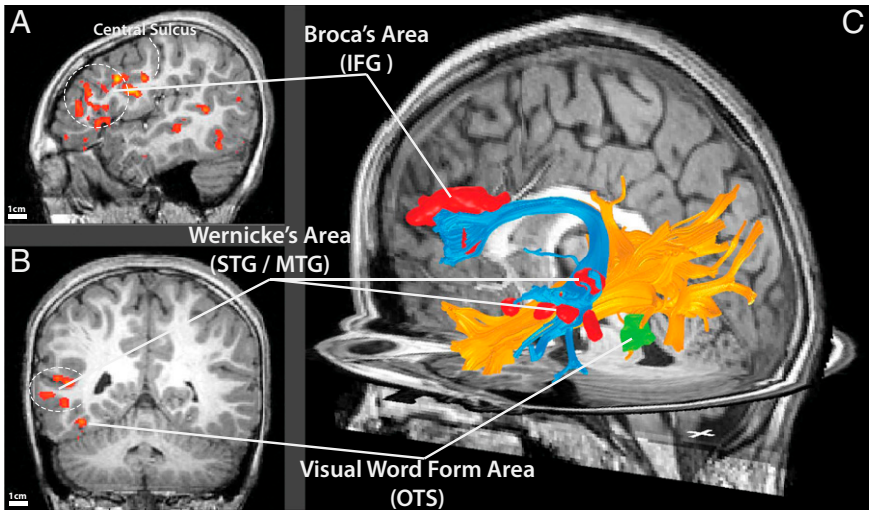

Fig. 1. Essential cortical circuits and white-matter connections for reading. (*A* and *B*) Blood oxygen level-dependent responses in a 10-y-old engaged in a rhyming task. In alternating 12-s blocks the subject judged if a pair of written words rhyme or whether two line patterns are the same. The subject's gray matter was segmented, and regions within the cortex with reliable task-related modulations ($P < 0.001$, uncorrected) were identified (colored overlay). A sagittal and coronal plane are shown to illustrate the phonological processing-related activations in the inferior frontal gyrus (IFG; Broca's area) and superior/middle temporal gyrus (STG/MTG; Wernicke's area) and the orthographic processing-related activation in the occipito-temporal sulcus (OTS). (*C*) Responsive voxels from Broca's area and Wernicke's area were rendered in 3D and displayed as surfaces within the brain volume (red). Two large fascicles, estimated with deterministic fiber tractography, are shown also. The arcuate fasciculus (blue) may carry phonological signals from the posterior temporal lobe to the inferior frontal lobe. The VWFA activation is rendered as a green surface. The ILF (orange) may carry signals from the VWFA to the anterior and medial temporal lobe. Fig. S7 shows the procedure used to identify the arcuate and ILF.

Diffusion properties of the arcuate and ILF changed from year to year: Children with the highest fractional anisotropy (FA) (*Methods*) in the first sample measurement did not have the highest FA the next year. Hence we measured the developmental trajectory (rate of change) of these pathways in each child across the 3 y of this study. We can summarize the pathway development by two numbers, the FA starting point and the rate of change. To relate brain measurements to behavioral performance, we measured the relationship between pathway-development parameters and reading skill.

Diffusivity Development in the Arcuate and ILF. We identified the left arcuate in 34 children and the left ILF in 39 children at three or more time points. FA values in the arcuate and ILF change between the ages of 7 and 15 y, and the rate of change over time varies among children (Fig. 2).

To test for a relationship between slope of FA and age, we fit a linear model to each child's four FA measurements. The linear model estimates each pathway's change in FA over time. For each child we obtain a slope (a) and intercept (b). The slope describes the average change year to year; the intercept is the estimated FA at an age of zero.

$$FA = (Age) \times a + b$$

For each child, the change in FA values over time is approximately linear from the age of 7–15 y. The key evidence supporting this observation is that linear slope estimates do not correlate significantly with the child's age at enrollment (Fig. S1). If the rate of change in FA declined in the later years because of nonlinear development, we would expect that the slopes of the older children would be less

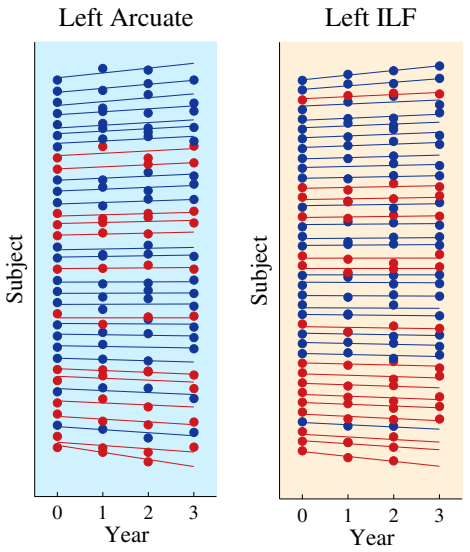

Fig. 2. Development rates in left arcuate and left ILF vary among children. Each child's FA development was characterized by a line, FA = (Age)*a + b. The FA measurement at each time point is the average across the fiber tract. The individual lines are shifted with respect to the vertical axis and are ordered based on the estimated slope. The lines also are aligned horizontally to coregister with the measurement date. There is no systematic relationship between a child's absolute age and the development rate, suggesting that each child has a linear developmental trend spanning the 7–15 y age range (Fig. S1). Data from children with above-average reading scores are shown in blue, and data from children with below-average reading scores are shown in red. Children with above-average reading scores tend to have positive development rates, and children with below average scores tend to have negative rates.

Table 1. Rank order correlations (Spearman) among children's Woodcock–Johnson Basic Reading scores in different years

	Year 1	Year 2	Year 3	Year 4
Year 1	1	0.86	0.79	0.84
Year 2		1	0.85	0.90
Year 3			1	0.89
Year 4				1

steep than the slopes of the younger children. The correlation between age and FA slope for the arcuate is $r = 0.06$ ($P = 0.71$) and for the ILF is $r = -0.23$ ($P = 0.14$). The mean FA slopes for the younger and older halves of the sample are essentially the same: 0.03×10^{-3} (FA/y) and 1.8×10^{-3}, $t = -0.8$ ($P = 0.48$) for the left arcuate and 0.34×10^{-3} and -0.04×10^{-3}, $t = 0.28$ ($P = 0.78$) for the left ILF.

We further tested the possibility of departures from linear development by fitting mixed-effects models with linear, quadratic, and cubic developmental effects. The models with nonlinear terms did not explain additional variance beyond the linear model (*SI Text*, *Linearity of FA Development*). Hence between 7 and 15 y of age FA development of the arcuate and ILF are very close to linear. This result is consistent with previous reports (e.g., ref. 16) (Fig. 1).

The implication is that a child's FA slope in any 3-y period from age 7–15 y is equivalent. The absence of a correlation between age and slope suggests that the variance in the developmental trajectories of the arcuate and ILF is explained by factors other than age.

Individual slope estimates were normally distributed with a relatively small mean and large SD for both the arcuate (0.92×10^{-3} FA/y $\pm$ 6.5×10^{-3}) and the ILF ($0.15 \times 10^{-3} \pm 4.0 \times 10^{-3}$). A group analysis of the change in FA at these ages, of the sort one would obtain in a cross-sectional study, shows very slightly positive change. However, the data from individual subjects are highly reliable, and the change in FA varies significantly among individuals (Fig. 2). Some children showed positive linear change in FA, others showed stable FA, and some children showed a linear decrease in FA across the four measurement times. Hence, there is very meaningful variation in developmental trends among subjects that is not observable in cross-sectional studies. Although the group mean is slightly positive, roughly one third of the subjects showed consistent declines across the four measurement periods.

To quantify the magnitude of FA change, we compared the changes observed in individual children with the changes in the arcuate and ILF of two adults measured on multiple occasions. The adult data assess the scanner stability and accuracy of the processing methods but also include any biological variation in the adult brain over the period of the measurements. Therefore, this analysis is a conservative estimate of the instrumental and processing noise. We performed a bootstrap analysis of linear fits to the adult data to generate a distribution of slopes that would be expected based on instrumental variation. The change in FA measured in many of the children was well outside the 95% confidence interval (CI) of slopes derived from the repeated adult measurements. For the left arcuate, 15 children had slopes more than 2 SD above zero, 9 children had slopes more than 2 SD below zero, and 10 children were within 2 SD of zero. For the ILF, 15 children had slopes more than 2 SD above zero (positive), 14 children had slopes more than 2 SD below zero (negative), and 10 children were within 2 SD of zero (zero). We refer to these groups as the "significant positive change," "significant negative change," and "no-change" groups.

Individual Differences in Reading Skill Correlate Positively with FA-Development Rate in Left Arcuate and ILF. Reading skills explained a significant portion of the variation in left arcuate growth rates ($r = 0.40$, bootstrap 95% CI = 0.13–0.67, $P = 0.02$): Above-average readers tended to have positive slopes, whereas below-average readers tended to have negative slopes (Fig. 3*A*, Fig. S2,

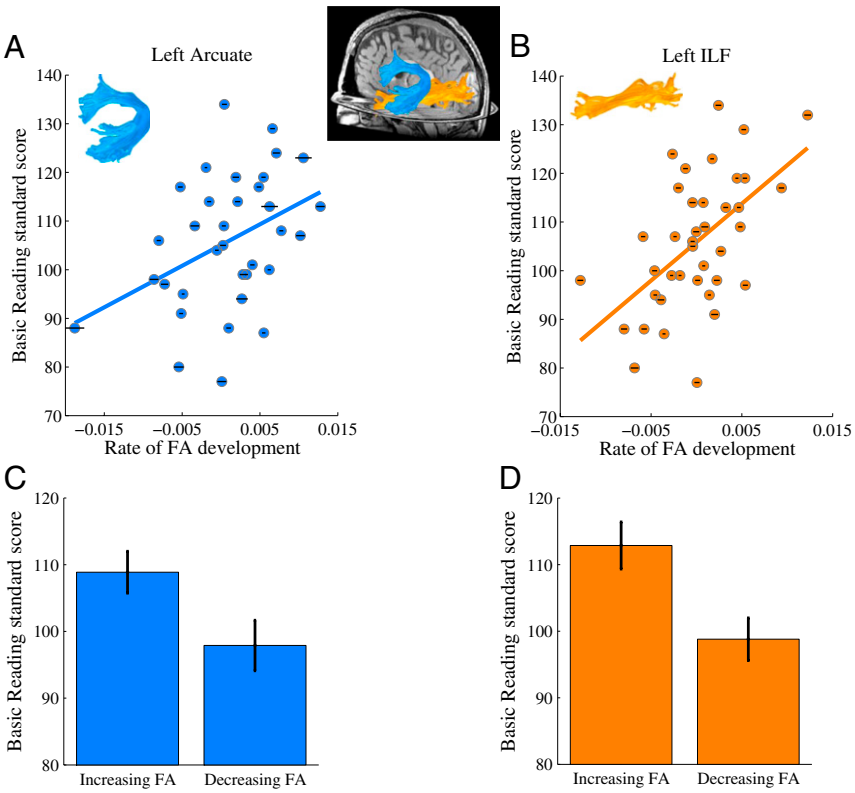

Fig. 3. Rate of FA development for left arcuate and left ILF correlates with reading skills. (*A* and *B*) The FA-development rate correlates positively with reading skills (Basic Reading, Woodcock–Johnson) for both the left arcuate (*A*) and the left ILF (*B*). Results are equivalent when reading skills are averaged across the four measurements (Fig. S2). The small horizontal black bars within the points are 95% CIs (1,000 bootstrap replications) for each child's estimated slope. The magnitude of the correlation for the left arcuate remains essentially same ($r = 0.40$ versus $r = 0.39$) when the subject with the lowest slope estimate is removed. (*Inset*) The arcuate and ILF from a typical subject. (*C* and *D*) In both tracts reading scores are significantly lower in children with FA-development slopes significantly below zero ($n = 9$ arcuate, $n = 14$ ILF) than in children with slopes significantly above zero ($n = 15$ arcuate, $n = 15$ ILF). The data for this figure and additional characteristics of the individual subjects are given in Dataset S1.

and Dataset S1). This correlation was consistent across multiple measures of reading skills including untimed single word reading (Woodcock–Johnson), timed single-word reading (TOWRE), and timed passage reading (GORT). The correlations remained significant when the manually segmented tracts were used instead of automatically segmented tracts (*Methods*) and when the sample was limited to the children with 4 y of data. Using a linear mixed-effects model, we confirmed that the rate of FA change over time in the left arcuate covaries with children's relative proficiency at single-word reading (*SI Text*, *Interaction of FA-Development Rate in Arcuate and ILF with Reading Skill*). Furthermore the children with significant positive change in the left arcuate were significantly better readers than children with significant negative change in the left arcuate ($T = 2.2$, $P < 0.05$) (Fig. 3*C*). The following analyses focus on the Woodcock–Johnson Basic Reading Skills Composite Index because it is the most commonly used reading assessment. Results for other measures are shown in the *SI Text*.

Reading skills also explained a significant portion of the variation in left ILF growth rates ($r = 0.51$, bootstrap 95% CI = 0.31–0.76, $P < 0.01$) (Fig. 3*B*). Using a linear mixed-effects model, we confirmed that the rate of FA change over time in the left ILF covaries with children's relative proficiency at single-word reading (*SI Text*). Furthermore the children with significant positive change in the left ILF were significantly better readers than children with significant negative change in the left ILF ($T = 2.9$, $P < 0.01$) (Fig. 3*D*).

A more subtle result that would be of interest is detecting an association between the rate of reading development and the rate of white-matter development. Such a correlation could arise if reading progress differed substantially among subjects. However, the rate of reading improvement was similar among subjects: Poor and good readers both improved, with few changes in rank order. There was no relationship between the rate of change in reading skills across the four measurements (measured with raw scores or standardized scores) and the rate of change in FA for either pathway. The absence of a correlation between these two rates does not imply that there are no biological changes associated with changes in reading ability. It only means that the rate at which readers improve is similar, and thus the statistical power for detecting a covariation between the two rates is low.

Correlations Are both Anatomically and Behaviorally Specific. The relationship between white-matter development and reading was specific to the left arcuate and left ILF. We fit the same developmental models for the right hemisphere homologs of these pathways and found no systematic relationship between reading skills and white-matter properties (Fig. S3). A bootstrap analysis confirmed that the correlation between FA change and reading skills was significantly greater for the left ILF than for the right ILF in more than 99% of the bootstrap samples. The bootstrap correlation of the left arcuate exceeded that of the right arcuate 85% of the time. We could identify the right arcuate in only 20 of the subjects, so the statistical power for comparisons including this tract is modest.

We further identified two tracts in both the left and right hemispheres to serve as comparison tracts: (*a*) the corona radiata and (*b*) the anterior thalamic radiations. Both pathways project to subcortical structures. The rates of FA development in these tracts varied; however, there was no covariation with reading skills (Fig. S3).

The anterior thalamic radiations are not normally considered candidates for explaining reading development and serve as control for general brain development. A bootstrap analysis confirmed that the correlation was greater for the reading pathways (left arcuate and left ILF) than for the anterior thalamic radiations in more than 99% of the bootstrap samples.

Niogi et al. (10) reported a relationship between reading and FA in the corona radiata, which we were not able to find (6), so we decided to re-examine this pathway. A bootstrap analysis confirmed that the correlation was greater for the left ILF than for the corona radiata in more than 99% of the bootstrap samples. The correlation was greater for the left arcuate than for the left corona radiata in 93% of the samples.

Hence, the measured correlations between tract FA development and reading skill are specific to the fiber bundles that connect the principal cortical circuits for reading; the correlations are not the result of general brain maturation.

To test the behavioral specificity of the reading correlations, we measured the covariation between left arcuate and left ILF development and the Wechsler Intelligence Scale for Children (WISC) full-scale IQ (30). Even though reading skills and IQ are highly correlated ($r = 0.53$, $P < 0.01$), there was no relationship between IQ and pathway development (Fig. S4). A bootstrap analysis confirmed that for the left ILF, the FA slope correlation with reading was higher than the correlation with IQ in more than 99% of the bootstrap samples. For the left arcuate the correlation with reading was higher than the correlation with IQ in 92% of the bootstrap samples. These analyses confirm that covariation between reading skills and white-matter maturation of these specific fascicles is specific to reading. The left arcuate and left ILF do not develop particularly rapidly in a child who scores high on IQ measures unless the child also is specifically talented at reading.

Individual Differences in Reading Skill Correlate Negatively with Initial FA in the Left Arcuate and Left ILF. Reading skills were negatively correlated with estimated intercepts for the left arcuate ($r = -0.40$, bootstrap 95% CI = −0.60 to −0.14, $P = 0.02$): Above-average readers had lower initial FA than below-average readers (Fig. 4, *Left* and Fig. S5). Reading skills also were negatively correlated with estimated intercepts for the left ILF ($r = -0.49$, bootstrap 95% CI = −0.70 to −0.25, $P < 0.01$) (Fig. 4, *Right*). Once again there were no effects in right hemisphere homologs of these pathways or in the four sensory-motor control pathways that we measured. For the control pathways, growth rates and intercepts varied among subjects, but neither rates nor intercepts covaried with reading skills.

Divergent Developmental Trajectories Between Above-Average and Below-Average Readers. Above-average readers start at significantly lower FA in the left arcuate and left ILF, and FA increases over time. Below-average readers start at significantly higher FA in the left arcuate and ILF, and FA decreases over time. We summarize the results by averaging development estimates for above-average readers (Basic Reading Skills >50th percentile) and below-average readers (Basic Reading Skills <50th percentile) (Fig. 5). There were 11 female and 13 male above-average readers (mean age 9.6 y) and eight female and seven male below-average readers (mean age 9.7 y). Above-average and below-average readers differed significantly on all measurements of reading skills at all time points in the study (Table S1).

At the first sample point, below-average readers had higher FA than above-average readers. In the middle of the sampled age range the above-average and below-average readers had equivalent FA. Finally, as the children matured the FA differences reappeared, with the above-average readers having higher FA than the below-average readers. Hence, the likelihood of observing an FA difference as a function of reading skill depends on the age at which a child is measured. Reading skills are better predicted by the rate of FA development than by the instantaneous FA level at any given age. A longitudinal study design is essential for this discovery.

Combining FA-Development Rates from the Left Arcuate and Left ILF Accurately Predicts Basic Reading Scores. Reading requires efficient phonological as well as orthographic processing. Therefore, we investigated whether left arcuate and left ILF development contribute independently to predicting reading skills. We used an additive regression model to predict reading scores as a function

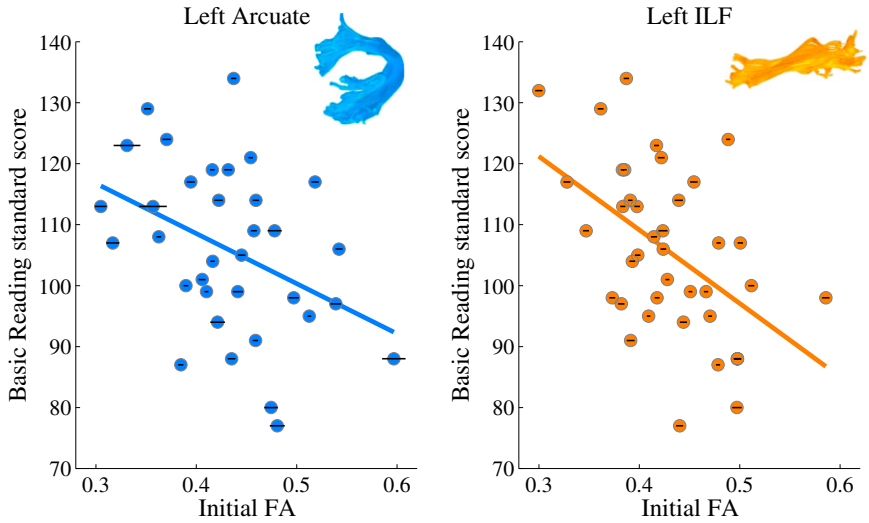

Fig. 4. Initial FA for left arcuate and left ILF correlates negatively with reading skills. The FA intercept correlates negatively with reading skills for the left arcuate and left ILF. The small horizontal black bars within the points are 95% CIs (1,000 bootstrap replications) estimated for each child's estimated intercept. Results are equivalent when reading skills are averaged across the four measurements (Fig. S5).

of estimated arcuate and ILF growth rates. Arcuate and ILF growth rates were not correlated ($r = 0.06$, $P = 0.69$), and within the additive model both were significant positive predictors of reading. The additive model accounted for 43% of the variance in reading scores, and the contribution of each tract was equivalent (Fig. 6). This result suggests that the development of the two pathways differentially influence aspects of reading development. FA-development rates also predict scores on other independent measurements of reading skills (Fig. S6).

Discussion

Neurobiology of White-Matter Development and Changes in the Diffusion Signal. During prenatal development, long-range axonal connections are guided to their cortical targets by molecular signaling mechanisms (31). Beginning in the late prenatal period and continuing through infancy and childhood, oligodendrocytes wrap myelin around these axons. This myelination process depends on both intrinsic genetic codes and extrinsic environmental factors (32). The myelination process is plastic; the level of electrical activity of an axon influences myelination (33, 34).

Myelination speeds signal conduction between distant cortical regions; however, the axons occupy more space, because each wrap of myelin increases the outer diameter of the axon. During development, some axons grow, and other axons are eliminated in a process called "pruning" (35, 36). LaMantia and Rakic (35) demonstrated that a rhesus monkey's corpus callosum contains 3.5 times more axons at birth than in adulthood. The pruning process also is driven in part by experience (37). Underused axons are pruned away during childhood, and the remaining axons are increasingly myelinated. Both myelination and pruning occur in the adult brain (34, 37), but both processes are more active during development.

Both these developmental changes influence the diffusion properties measured in the fascicle. Myelination increases the space occupied by axons in a voxel, leading to increased FA (38), whereas the removal of superfluous axons decreases the space occupied by axons, leading to decreased FA. The effects of axon density and myelination on diffusion measurements have been confirmed in animal models: Both demyelination and axon degeneration lead to decreases in diffusion anisotropy, and anisotropy returns to normal as the tissue regenerates (39–42; for a review see ref. 43). Similar effects have been reported in humans. For example in patients with focal infarcts in the posterior limb of the internal capsule, axon loss leads to decreases in diffusion anisotropy along the full length of the motor pathway (44). Several biological factors influence FA; the mechanisms of myelination and pruning are among the leading candidates for explaining the FA changes over time in our data.

Cross-sectional diffusion tensor imaging (DTI) studies of white-matter development have outlined the average developmental trajectory for most major fascicles (16, 17, 45). However, because both processes are influenced by experience and learning, there must be considerable biological variability in the rate and timing of growth and pruning. Individual variability in these processes may contribute to differences in cognitive development, such as reading abilities.

Dual-Process Account of White-Matter Development. What might be the white-matter biology that produces the observed developmental changes in the diffusion measurements? Given that white-matter maturation depends on at least two opposing processes—myelination and pruning—we might consider a phenomenological dual-process model of development. We illustrate a set of FA-development curves based on the same formula that characterizes the critical damping in many homeostatic systems (Fig. 7). The simulation illustrates how a dual-process system with one process, e.g., myelination, that increases FA and a second process, e.g., pruning, that decreases FA can produce the variation in developmental trajectories observed in our data.

In one case the two processes are synchronous throughout development, and the FA value increases monotonically and approaches its mature level. The presence of pruning at an early age dampens the rate of FA increase. In the second case, the processes are asynchronous. Early development is dominated by increasing FA, and at an early age the FA level exceeds the target level; later development is dominated by pruning, and FA decreases. This developmental model of homeostatic growth with asynchrony between the two processes is consistent with the observation that some subjects showed an increase in FA (blue dashed line in Fig. 7) and others a decrease (red dashed line in Fig. 7).

In these two developmental scenarios, the experiential factors governing development also differ. In the first scenario, when FA increases monotonically, the two processes are driven by the same experiential factors in the child's environment. In the second scenario, when FA overshoots the target, the process of FA increase is influenced by the experience at early ages, and the process of FA decrease is influenced by experience at later ages.

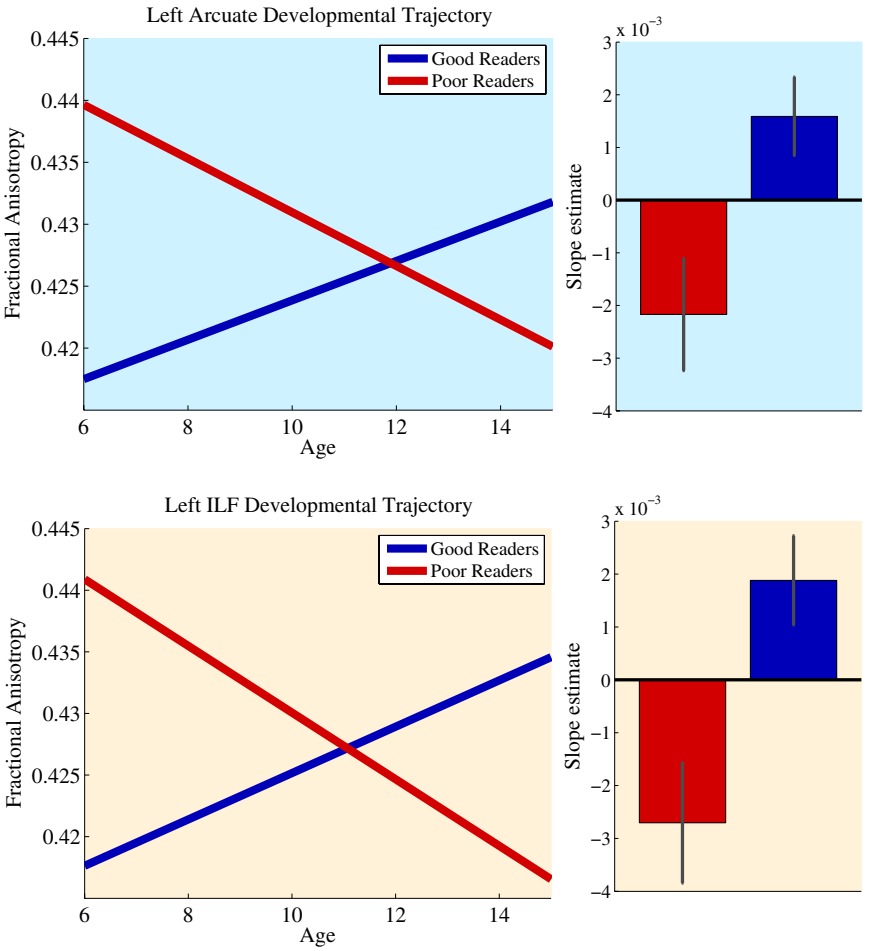

Fig. 5. White-matter development from age 7–15 y differs between above-average and below-average readers. Average development rates for above-average (blue) and below-average readers (red) were estimated by averaging the individual slope and intercept estimates within each group (group descriptive statistics reported in Table S1). The slopes differed significantly between groups ($P < 0.05$) for both the left arcuate (*Upper*) and left ILF (*Lower*). (*Left*) The mean developmental trajectory for each group. (*Right*) The mean developmental rate for the two groups in each pathway. Data shown are ± 1 SEM.

The data show that children with low initial FA and a positive FA slope are better readers than children with high initial FA and a negative FA slope. In the final stages of development, the FA levels are reversed: People with higher FA in specific tracts are better readers than people with lower FA. Hence, the dual-process model explains the different FA levels in the groups at the initial and final measurement points based on the relative timing of active developmental processes.

The specific idea that myelination and pruning are the driving processes cannot be tested from measurements presented here, but future longitudinal studies capitalizing on quantitative MRI measurements of tissue properties related to myelination can test the dual-process scenario in humans. Quantitative T1 and T2 mapping can be combined with biophysical tissue models to quantify the chemical properties of axonal membranes so as to assess the effects of myelination (46, 47), and quantitative proton density can quantify the amount of tissue within a voxel to assess the effects of pruning. Also, myelin water fraction (46) and bound pool fraction (38, 48) measure quantities that are weighted by myelination. Quantitative data also may allow us to test a completely different explanation, namely that the FA changes do not reflect tissue properties of the ILF and arcuate but instead are driven by the growth of fiber bundles crossing through these pathways. For example, an increase in the density of axons in a fiber bundle that crosses through the arcuate or ILF would account for the decreases in FA that we measured in these fascicles for the poor readers. High-angular-resolution diffusion imaging can measure the effects of crossing fibers by quantifying the relative weights on multiple fiber populations within a voxel (49, 50). An alternative explanation of the data, based on two processes that reflect neighboring pathway development, remains a real possibility.

Finally, what might be the causal factors driving the timing of the two processes? Variation in the quality of early-life language input, the differential effect of children's reading experience, the timing of instruction with respect to these processes, and genetic factors could all contribute.

Education and Plasticity: The Neural Basis of Learning to Read. Learning to read influences the development of the brain: Cerebral gray matter circuits and the white matter connecting them learn to extract the statistical regularities of text written in a person's native language (5). We hypothesized that learning to read depends in part on the capacity of white-matter pathways to develop in response to literacy training. We found that the rate of development of the arcuate and ILF covary with children's reading skills.

A significant challenge for neuroscientists is to characterize the conditions under which a specific neural circuit is plastic or stable and how the circuit's capacity for plasticity relates to the behavior of the organism. The brain matures in a sequential manner in which some circuits develop and stabilize while others remain capable of plastic change (51–54). In this view, reading instruction should be delivered when the systems needed to learn

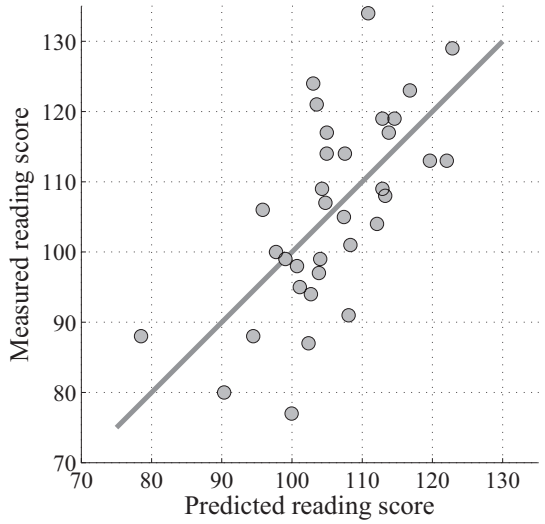

Fig. 6. Prediction of reading scores combining left arcuate and left ILF FA development. A linear combination of FA-development rate (slope) estimates for the left arcuate and left ILF predict 43% ($r = 0.66$) of the variance in measured Woodcock–Johnson Basic Reading standard scores. Predicted reading scores are shown on the horizontal axis, and measured scores are shown on the vertical axis. Left arcuate and ILF development predict other standardized measures of reading skill as well (Fig. S6).

the material are adequately developed but still have a potential for further plasticity so that they can respond to the instruction. The measurements we report provide an individualized time frame during which certain key white-matter pathways are developing. These data suggest that successfully learning to read requires coordinated development of key white-matter pathways.

Conclusion

Despite similar quality of education, there is wide variability in how efficiently children acquire essential academic skills. The rate at which a child learns to read early in elementary school is highly predictive of the person's relative reading proficiency throughout childhood, adolescence, and adulthood (55, 56). The stability of children's relative reading proficiency has motivated attempts to use neuroimaging measurements to predict children's educational outcomes (neuroprognosis), with the long-term goal of developing individualized education programs (57, 58). The measurements here show that there are active biological processes in specific white-matter tracts, that these processes differ among children, and that these differences correlate with reading skills. Future studies are needed to determine whether individual children benefit from instruction that is tailored and timed to the developmental processes measured here.

Methods

We followed children with a wide range of reading skills and ages in an accelerated longitudinal design (59). Four annual waves of longitudinal measurements included anatomical and functional MR scans as well as a battery of age-standardized cognitive tests.

Participants. The initial cohort included 55 children (30 girls, 25 boys), 7–12 y old. Demographics describing the participant population across the four sample points were published in ref. 2. Participants with a wide range of reading skills were recruited from the San Francisco Bay Area schools. Written informed consent/assent was obtained from both parents and children. All participants were physically healthy and had no history of neurological disease, head injury, psychiatric disorder, language disability [verified by the Clinical Evaluation of Language Fundamentals (CELF-3) screening test], attention deficit/hyperactivity disorder (verified by Conners' Parent Rating Scale-Revised Short Form), or depression (verified by the Children's Depression Inventory Short Form). All participants were native English speakers and had normal or corrected-to-normal vision and hearing. Participants were paid per session; they also received a brain picture and small merchandise items for their participation each year (a water bottle and a T-shirt with a brain logo). The Stanford Panel on Human Subjects in Medical and Non-Medical Research approved all procedures.

Subject attrition was about 20% each year. The principal reasons for attrition were (*a*) nonremovable dental braces, frequently installed around age 9–10 y, causing artifacts in MR images, and (*b*) loss of interest, particularly among the older children. Of the initial 55 participants, 28 remained with us for all four measurements. The 29th participant in measurement 4 could not participate in years 2 and 3 because of braces but returned for the fourth measurement when the braces were removed. Subjects who participated in at least three measurements ($n = 39$) were included in the present analysis. We further confirmed that every effect we report remained significant when the sample was limited to the 28 subjects with four complete measurements.

Procedure. Each year, starting in summer 2004 and ending in summer 2007, participants took part in three or four separate experimental sessions in the following order: cognitive assessment, anatomical MRI, and functional MRI (fMRI data are described in ref. 2). The anatomical MRI session included high-resolution T1-weighted spoiled gradient recalled (SPGR) scans and 12-direction DFI scans.

Cognitive Assessment. Participants were administered a comprehensive assessment of reading and reading-relevant cognitive skills that took approximately 4 h to complete. Tests were administered by an experienced neuropsychologist. In following years, a shortened 2-h assessment was administered. The assessment included the TOWRE (60), subtests from the Woodcock–Johnson–III Test of Achievement (29), subtests from CTOPP (61), and GORT-4 (62). All the reading measures were highly correlated. The analyses in this paper focus on the Woodcock–Johnson Basic Reading Skills composite index, which includes the Word Identification (an untimed measure of single-word reading accuracy) and Word Attack (an untimed measure of pseudoword reading accuracy) subtests. Results for other reading measures are reported in *SI Text*.

Intelligence was assessed by the WISC–IV (30), and general language was measured by CELF-3 screening text (63), both in the first year only. A full-

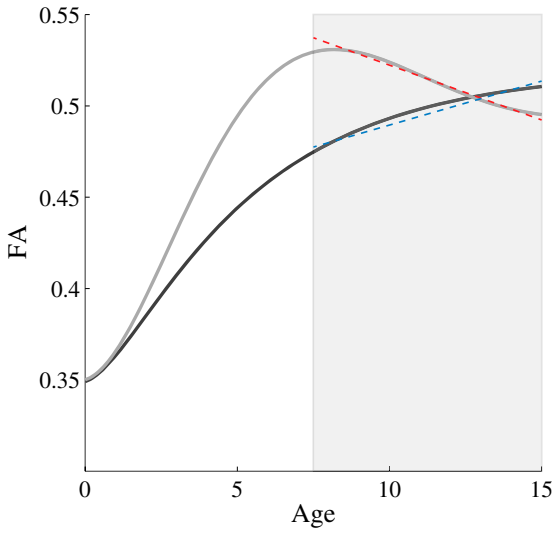

Fig. 7. A dual-process model of white-matter development. FA development with age is illustrated for two cases. In all children, white-matter tract FA is low at birth and increases with age. Tract development combines myelination and pruning of axons, and the balance between these processes differs among children. The balance between the two processes can be modeled by simple homeostatic equations that govern development over time; the parameters of the developmental processes were chosen to model the characteristics of the above-average readers (black curve) and below-average readers (gray curve). The model for the above-average group has synchronous development of the processes, whereas the below-average group is modeled with slightly asynchronous development. For both groups the FA developmental rate is approximately linear during the age range of 7–15 y (shaded region), but the specific rate of development differs (dotted lines).

scale intelligence quotient of at least 85 and a passing score on the CELF-3 screening test were required for inclusion.

Acquisition of Diffusion-Weighted Imaging Data. MRI data were acquired on a 1.5-T Signa LX scanner (Signa CVi; GE Medical Systems) using a self-shielded, high-performance gradient system. A standard quadrature head coil, provided by the vendor, was used for excitation and signal reception. Head motion was minimized by placing cushions around the head and securing a strap across the forehead.

The DTI protocol used eight repetitions of a 90-s whole-brain scan. The scans were averaged to improve signal quality. The pulse sequence was a diffusion-weighted single-shot spin-echo, echo planar imaging sequence (63 ms TE; 6 s TR; 260 mm FOV; 128 × 128 matrix size; ±110 kHz bandwidth; partial k-space acquisition). We acquired 60 axial, 2-mm-thick slices (no skip) for two b-values, b = 0 and b = 800 s/mm^2. The high b-value data were obtained by applying gradients along 12 diffusion directions (six noncollinear directions). Two gradient axes were energized simultaneously to minimize TE, and the polarity of the effective diffusion-weighting gradients was reversed for odd repetitions to reduce cross-terms between diffusion gradients and imaging and background gradients. Although Jones et al. (64) suggest that measuring more diffusion directions might be more efficient in reliably estimating diffusion tensors of arbitrary orientation, our signal-to-noise ratio is sufficiently high from our eight repeats to produce very reliable tensor estimates. We have confirmed this reliability in a subset of subjects by comparing bootstrapped tensor uncertainty estimates of the 12-direction data reported here with an additional 40-direction dataset that was acquired in each child in the third measurement year. With our high signal-to-noise ratio, tensor uncertainty is limited by physiological noise rather than measurement noise.

We also collected high-resolution T1-weighted anatomical images for each subject using an 8-min sagittal 3D-SPGR sequence (1 × 1 × 1 mm voxel size). The following anatomical landmarks were defined manually in the T1 images: the anterior commissure (AC), the posterior commissure (PC), and the midsagittal plane. With these landmarks, we used a rigid-body transform to convert the T1-weighted images to the conventional AC–PC aligned space.

Data Preprocessing. Eddy-current distortions and subject motion in the diffusion-weighted images were removed by a 14-parameter constrained nonlinear coregistration based on the expected pattern of eddy-current distortions given the phase-encode direction of the acquired data (65).

Each diffusion-weighted image was registered to the mean of the (motion-corrected) non–diffusion-weighted (b = 0) images using a two-stage coarse-to-fine approach that maximized the normalized mutual information. The mean of the non–diffusion-weighted images was aligned automatically to the T1 image using a rigid body mutual information algorithm. All raw images from the diffusion sequence were resampled to 2-mm^2 isotropic voxels by combining the motion correction, eddy-current correction, and anatomical alignment transforms into one omnibus transform and resampling the data using a trilinear interpolation algorithm based on code from SPM5 (66). An eddy-current intensity correction (65) was applied to the diffusion-weighted images at the resampling stage.

The rotation component of the omnibus coordinate transform was applied to the diffusion-weighting gradient directions to preserve their orientation with respect to the resampled diffusion images. The tensors then were fit using a robust least-squares algorithm designed to remove outliers from the tensor estimation step (67). We computed the eigenvalue decomposition of the diffusion tensor, and the resulting eigenvalues were used to compute the FA (68). The FA is the normalized SD of the three eigenvalues and indicates the degree to which the isodiffusion ellipsoid is anisotropic (i.e., one or two eigenvalues are larger than the mean of all three eigenvalues). The mean diffusivity is the mean of the three eigenvalues, which is equivalent to one-third of the trace of the diffusion tensor.

We confirmed that the DTI and T1 images were aligned to within a few millimeters in the regions of interest (ROI) for this study. This confirmation was done by manual inspection by one of the authors (R.F.D.). In regions prone to susceptibility artifacts, such as orbito-frontal and inferior temporal regions, the misalignment was somewhat larger because of uncorrected echo planar imaging distortions.

All the custom image processing software is available as part of our open-source mrDiffusion package in VISTASOFT (revision 2289), available for download from http://white.stanford.edu/software.

Data Analysis. Our primary objective was to test the hypothesis that plasticity in key white-matter fascicles is related to children's reading development. We focused on the left hemisphere arcuate fasciculus and ILF because these tracts project to cortical circuits that are believed to be essential for skilled reading (3, 5, 6). We used the right hemisphere homologs of these pathways as well as sensory-motor tracts as control pathways to assess the anatomical specificity of our findings. To detect changes in the tissue properties of these pathways reliably over the course of development, we developed and validated an automated procedure for segmenting each pathway in an individual's DTI data.

Fiber-Tract Identification. To identify the fiber tracts of interest reliably across subjects and measurements, we developed an atlas-based procedure based on Hua et al. (69) that segmented fiber tracts in each subject's native space in two steps. First we used deterministic tractography to estimate each subject's whole-brain fiber group. We seeded the tracking algorithm with a mask of all voxels with an FA value greater than 0.3 (70, 71). Fiber tracts were estimated using a deterministic streamlines tracking algorithm (STT) (70, 71) with a fourth-order Runge–Kutta path integration method and 1-mm fixed-step size. A continuous tensor field was estimated with trilinear interpolation of the tensor elements. Starting from initial seed points within the white-matter mask, the path integration procedure traced streamlines in both directions along the principal diffusion axes. Individual streamline integration was terminated using two standard criteria: Tracking was halted if (*a*) the FA estimated at the current position was below 0.15 or (*b*) the minimum angle between the last path segment and next step direction was >50°.

Fibers from the whole-brain fiber group described above were scored based on their similarity to a previously published fiber probability map (69) that quantified the likelihood that a particular voxel contains fibers from any particular fiber tract. This procedure identifies fibers as candidates for a particular fiber group if they follow a trajectory similar to that of the fiber groups identified in 28 healthy adults by Hua et al. (69). Next, regions of interest defined on an average brain were warped into each subject's native space based on a nonlinear transformation that aligned the average brain to the subject's b=0 volume (66). Each of the four fiber tracts was isolated by restricting the candidate fibers identified above to a pair of waypoint ROIs described in a white-matter atlas (72, 73). These waypoints have been shown to be accurate ways to isolate particular fiber groups (69, 73). We have found through comparison with manually segmented fiber tracts (described below) that the combination of the Hua et al. template scoring procedure and the waypoints ROI procedure produces better fiber group segmentations than produced by either method alone. Fig. S7 shows the automated segmentation procedure for the left arcuate fasciculus.

Fiber Group Development Estimates. We extracted the three tensor eigenvalues at 1-mm steps along each estimated fiber. From these, we calculated FA, mean diffusivity, radial diffusivity, and axial diffusivity and averaged each measure along the entire tract. This method effectively computed a weighted-average, because voxels with greater fiber density contributed more to the final measure than voxels with low fiber density. This weighting reduced the effects of partial voluming, because the fiber density is related to the likelihood that a voxel is filled with fibers from the tract of interest. Thus, each subject's fiber tract data were summarized with a single measurement for each year. The confidence interval of each year's measurement was estimated using a bootstrap procedure (74) with 1,000 iterations, in which we randomly sampled with replacement the fibers within the fiber group that were used to generate the average measurement. We used linear regression to fit a line that characterized each child's average change in FA over time for the 4-y period of the study. We included all children who had at least three data points. The error of each subject's slope of FA change was estimated as the SD of the slope estimates from the linear fit to each bootstrap sample.

We confirmed the robustness of the measurements in two ways. First a trained experimenter (J.D.Y.) manually segmented the left hemisphere arcuate fasciculus fiber group in each subject's year 1 DTI data based on the method described by Yeatman et al. (6). Manual segmentation remains the gold standard for accurate identification of white-matter fascicles. The diffusion measurements obtained for the manual versus the automated segmentations of the 55 subjects were highly correlated, confirming the accuracy of the automated procedure (r = 0.85 for FA, r = 0.95 for radial diffusivity, and r = 0.82 for axial diffusivity values). Second, the voxels identified in the year 1 manual segmentations were used as an ROI across the 4 y, and diffusion measurements within these voxels were averaged for each year's data to estimate change over time in a consistent set of voxels. All findings reported in this paper remained significant when the manual segmentation ROIs from y 1 were used to compute tract statistics.

ACKNOWLEDGMENTS. This work was supported by National Institutes of Health Grant R01 EY015000 (to B.A. W.). J.D.Y. is the recipient of a National Science Foundation Graduate Research Fellowship.

1. Geschwind N (1965) Disconnexion syndromes in animals and man. II. *Brain* 88(3): 585–644.
2. Ben-Shachar M, Dougherty RF, Deutsch GK, Wandell BA (2011) The development of cortical sensitivity to visual word forms. *J Cogn Neurosci* 23(9):2387–2399.
3. Wandell BA (2011) The neurobiological basis of seeing words. *Ann N Y Acad Sci* 1224: 63–80.
4. Dehaene S, et al. (2010) How learning to read changes the cortical networks for vision and language. *Science* 330(6009):1359–1364.
5. Wandell BA, Rauschecker AM, Yeatman JD (2012) Learning to see words. *Annu Rev Psychol* 63:31–53.
6. Yeatman JD, et al. (2011) Anatomical properties of the arcuate fasciculus predict phonological and reading skills in children. *J Cogn Neurosci* 23(11):3304–3317.
7. Yeatman JD, Rauschecker AM, Wandell BA (2012) Anatomy of the visual word form area: Adjacent cortical circuits and long-range white matter connections. *Brain Lang*, in press.
8. Rauschecker AM, et al. (2009) Reading impairment in a patient with missing arcuate fasciculus. *Neuropsychologia* 47(1):180–194.
9. Epelbaum S, et al. (2008) Pure alexia as a disconnection syndrome: New diffusion imaging evidence for an old concept. *Cortex* 44(8):962–974.
10. Niogi SN, McCandliss BD (2006) Left lateralized white matter microstructure accounts for individual differences in reading ability and disability. *Neuropsychologia* 44(11): 2178–2188.
11. Beaulieu C, et al. (2005) Imaging brain connectivity in children with diverse reading ability. *Neuroimage* 25(4):1266–1271.
12. Deutsch GK, et al. (2005) Children's reading performance is correlated with white matter structure measured by diffusion tensor imaging. *Cortex* 41(3):354–363.
13. Klingberg T, et al. (2000) Microstructure of temporo-parietal white matter as a basis for reading ability: Evidence from diffusion tensor magnetic resonance imaging. *Neuron* 25(2):493–500.
14. Darki F, Peyrard-Janvid M, Matsson H, Kere J, Klingberg T (2012) Three dyslexia susceptibility genes, DYX1C1, DCDC2, and KIAA0319, affect temporo-parietal white matter structure. *Biol. Psychiatry* 72(8):671–676.
15. Yeatman JD, Feldman HM (2012) Neural plasticity after pre-linguistic injury to the arcuate and superior longitudinal fasciculi. *Cortex*, in press.
16. Lebel C, Walker L, Leemans A, Phillips L, Beaulieu C (2008) Microstructural maturation of the human brain from childhood to adulthood. *Neuroimage* 40(3):1044–1055.
17. Eluvathingal TJ, Hasan KM, Kramer L, Fletcher JM, Ewing-Cobbs L (2007) Quantitative diffusion tensor tractography of association and projection fibers in normally developing children and adolescents. *Cereb Cortex* 17(12):2760–2768.
18. Barnea-Goraly N, et al. (2005) White matter development during childhood and adolescence: A cross-sectional diffusion tensor imaging study. *Cereb Cortex* 15(12): 1848–1854.
19. Ashtari M, et al. (2007) White matter development during late adolescence in healthy males: A cross-sectional diffusion tensor imaging study. *Neuroimage* 35(2):501–510.
20. Coltheart M, Rastle K, Perry C, Langdon R, Ziegler J (2001) DRC: A dual route cascaded model of visual word recognition and reading aloud. *Psychol Rev* 108(1):204–256.
21. Jobard G, Crivello F, Tzourio-Mazoyer N (2003) Evaluation of the dual route theory of reading: A meta-analysis of 35 neuroimaging studies. *Neuroimage* 20(2):693–712.
22. Booth JR, et al. (2004) Development of brain mechanisms for processing orthographic and phonologic representations. *J Cogn Neurosci* 16(7):1234–1249.
23. Wagner R, Torgesen J (1987) The Nature of Phonological Processing and Its Causal Role in the Acquisition of Reading Skills. *Psychol Bull* 101:192–212.
24. Vandermosten M, et al. (2012) A tractography study in dyslexia: Neuroanatomic correlates of orthographic, phonological and speech processing. *Brain* 135(Pt 3): 935–948.
25. Rolheiser T, Stamatakis EA, Tyler LK (2011) Dynamic processing in the human language system: Synergy between the arcuate fascicle and extreme capsule. *J Neurosci* 31(47):16949–16957.
26. Gaillard R, et al. (2006) Direct intracranial, FMRI, and lesion evidence for the causal role of left inferotemporal cortex in reading. *Neuron* 50(2):191–204.
27. Cohen L, et al. (2003) Visual word recognition in the left and right hemispheres: Anatomical and functional correlates of peripheral alexias. *Cereb Cortex* 13(12): 1313–1333.
28. Dehaene S, Le Clec'H G, Poline JB, Le Bihan D, Cohen L (2002) The visual word form area: A prelexical representation of visual words in the fusiform gyrus. *Neuroreport* 13(3):321–325.
29. Woodcock RW, McGrew KS, Mather N (2001) *Woodcock Johnson-III Tests of Achievement* (Riverside Publishing, Itaska, IL).
30. Wechsler D (2003) *Wechsler intelligence scale for children* (Psychological Corporation, San Antonio, TX), 4th Ed.
31. Goodman CS, Shatz CJ (1993) Developmental mechanisms that generate precise patterns of neuronal connectivity. *Cell* 72(Suppl):77–98.
32. Emery B (2010) Regulation of oligodendrocyte differentiation and myelination. *Science* 330(6005):779–782.
33. Barres BA, Raff MC (1993) Proliferation of oligodendrocyte precursor cells depends on electrical activity in axons. *Nature* 361(6409):258–260.
34. Ishibashi T, et al. (2006) Astrocytes promote myelination in response to electrical impulses. *Neuron* 49(6):823–832.
35. LaMantia AS, Rakic P (1990) Axon overproduction and elimination in the corpus callosum of the developing rhesus monkey. *J Neurosci* 10(7):2156–2175.
36. LaMantia AS, Rakic P (1994) Axon overproduction and elimination in the anterior commissure of the developing rhesus monkey. *J Comp Neurol* 340(3):328–336.
37. Yamahachi H, Marik SA, McManus JN, Denk W, Gilbert CD (2009) Rapid axonal sprouting and pruning accompany functional reorganization in primary visual cortex. *Neuron* 64(5):719–729.
38. Stikov N, et al. (2011) Bound pool fractions complement diffusion measures to describe white matter micro and macrostructure. *Neuroimage* 54(2):1112–1121.
39. Beaulieu C, Does MD, Snyder RE, Allen PS (1996) Changes in water diffusion due to Wallerian degeneration in peripheral nerve. *Magn Reson Med* 36(4):627–631.
40. Stanisz GJ, Midha R, Munro CA, Henkelman RM (2001) MR properties of rat sciatic nerve following trauma. *Magn Reson Med* 45(3):415–420.
41. Budde MD, et al. (2008) Axonal injury detected by in vivo diffusion tensor imaging correlates with neurological disability in a mouse model of multiple sclerosis. *NMR Biomed* 21(6):589–597.
42. Song S-K, et al. (2002) Dysmyelination revealed through MRI as increased radial (but unchanged axial) diffusion of water. *Neuroimage* 17(3):1429–1436.
43. Beaulieu C (2002) The basis of anisotropic water diffusion in the nervous system - a technical review. *NMR Biomed* 15(7-8):435–455.
44. Pierpaoli C, et al. (2001) Water diffusion changes in Wallerian degeneration and their dependence on white matter architecture. *Neuroimage* 13(6 Pt 1):1174–1185.
45. Ben Bashat D, et al. (2005) Normal white matter development from infancy to adulthood: Comparing diffusion tensor and high b value diffusion weighted MR images. *J Magn Reson Imaging* 21(5):503–511.
46. Deoni SC (2010) Quantitative relaxometry of the brain. *Top Magn Reson Imaging* 21 (2):101–113.
47. MacKay A, et al. (1994) In vivo visualization of myelin water in brain by magnetic resonance. *Magn Reson Med* 31(6):673–677.
48. Yarnykh VL, Yuan C (2004) Cross-relaxation imaging reveals detailed anatomy of white matter fiber tracts in the human brain. *Neuroimage* 23(1):409–424.
49. Tuch DS, Reese TG, Wiegell MR, Wedeen VJ (2003) Diffusion MRI of complex neural architecture. *Neuron* 40(5):885–895.
50. Jeurissen B, Leemans A, Tournier JD, Jones DK, Sijbers J (2012) Investigating the prevalence of complex fiber configurations in white matter tissue with diffusion magnetic resonance imaging. *Hum Brain Mapp*, in press.
51. Smirnakis SM, et al. (2005) Lack of long-term cortical reorganization after macaque retinal lesions. *Nature* 435(7040):300–307.
52. Wandell BA, Smirnakis SM (2009) Plasticity and stability of visual field maps in adult primary visual cortex. *Nat Rev Neurosci* 10(12):873–884.
53. Norcia AM, Tyler CW (1985) Spatial frequency sweep VEP: Visual acuity during the first year of life. *Vision Res* 25(10):1399–1408.
54. Flechsig P (1901) Developmental (myelogenetic) localisation of the cerebral cortex in the human subject. *Lancet* 2:1027–1029.
55. Francis DJ, Shaywitz SE, Stuebing KK, Shaywitz BA, Fletcher JM (1996) Developmental lag versus deficit models of reading disability: A longitudinal, individual growth curves analysis. *J Educ Psychol* 88:3–17.
56. Torgesen J (1998) Catch them before they fall: Identification and assessment to prevent reading failure in young children. *Am Educ* 22:32–39.
57. Hoeft F, et al. (2011) Neural systems predicting long-term outcome in dyslexia. *Proc Natl Acad Sci USA* 108(1):361–366.
58. McNorgan C, Alvarez A, Bhullar A, Gayda J, Booth JR (2011) Prediction of reading skill several years later depends on age and brain region: Implications for developmental models of reading. *J Neurosci* 31(26):9641–9648.
59. Willett JB, Singer JD, Martin NC (1998) The design and analysis of longitudinal studies of development and psychopathology in context: Statistical models and methodological recommendations. *Dev Psychopathol* 10(2):395–426.
60. Torgesen J, Wagner R, Rashotte CA (1999) *Test of Word Reading Efficiency* (PRO-ED Publishing, Inc., Austin, TX).
61. Wagner R, Torgesen J, Rashotte CA (1999) *Comprehensive Test of Phonological Processes (CTOPP)* (Pro-Ed, Austin, TX).
62. Wiederholt JL (2001) *Gray Oral Reading Test-4th Edition (GORT-4)*. (Pro-Ed Publishing, Inc., Austin, TX).
63. Semel E, Wiig EH, Secord WA (1995) *Clinical Evaluation of Language Fundamentals 3 (CELF-3)* (The Psychological Corporation, San Antonio, TX).
64. Jones DK (2004) The effect of gradient sampling schemes on measures derived from diffusion tensor MRI: A Monte Carlo study. *Magn Reson Med* 51(4):807–815.
65. Rohde GK, Barnett AS, Basser PJ, Marenco S, Pierpaoli C (2004) Comprehensive approach for correction of motion and distortion in diffusion-weighted MRI. *Magn Reson Med* 51(1):103–114.
66. Friston KJ, Ashburner J (2004) Generative and recognition models for neuroanatomy. *Neuroimage* 23(1):21–24.
67. Chang LC, Jones DK, Pierpaoli C (2005) RESTORE: Robust estimation of tensors by outlier rejection. *Magn Reson Med* 53(5):1088–1095.
68. Basser PJ, Pierpaoli C (1996) Microstructural and physiological features of tissues elucidated by quantitative-diffusion-tensor MRI. *J Magn Reson B* 111(3):209–219.
69. Hua K, et al. (2008) Tract probability maps in stereotaxic spaces: Analyses of white matter anatomy and tract-specific quantification. *Neuroimage* 39(1):336–347.
70. Basser PJ, Pajevic S, Pierpaoli C, Duda J, Aldroubi A (2000) In vivo fiber tractography using DT-MRI data. *Magn Reson Med* 44(4):625–632.
71. Mori S, Crain BJ, Chacko VP, van Zijl PC (1999) Three-dimensional tracking of axonal projections in the brain by magnetic resonance imaging. *Ann Neurol* 45(2):265–269.
72. Mori S, Wakana S, van Zijl PC, Nagae-Poetscher LM (2005) *MRI Atlas of Human White Matter* (Elsevier, Amsterdam, Netherlands).
73. Wakana S, et al. (2007) Reproducibility of quantitative tractography methods applied to cerebral white matter. *Neuroimage* 36(3):630–644.
74. Effron B, Tibshirani RJ (1993) *An Introduction to the Bootstrap* (Chapman & Hall/CRC, Boca Raton, FL).